Chapter 5:
Hydrogen Storage Properties of the Pristine, Defected and Metal Decorated o-B_2N_2 Monolayer

5.1 Introduction

The scientific community is currently engaged in a pursuit to uncover an enhanced alternative to conventional fuels, driven by two primary factors: the exhaustion of finite energy reservoirs and their adverse environmental impacts. These effects encompass the deterioration of the ozone layer, brought about by phenomena like climate change and the release of harmful emissions.[1] A potential substitute worth considering is hydrogen, which stands out for its eco-friendliness and lack of pollution. When hydrogen is burned, it generates only water and warmth, without emitting any detrimental compounds like poisonous gases. This quality makes hydrogen a viable solution for mitigating environmental damage caused by traditional fuel sources.[2] Hydrogen possesses greater energy density than other fossil fuels and is employed as a power source for transportation vehicles.[3] The main obstacle involves the secure retention of hydrogen for use as fuel. Hydrogen storage can be divided into three key types: gaseous, liquid and solid. Storing hydrogen in its gaseous state raises safety issues and mandates the utilization of sizable and high-pressure containers.[4] Furthermore, the high expenses of liquefaction make liquid phase storage unfavourable.[5] However, holding hydrogen in solid form is a more efficient and meaningful option because it requires less volume.[6] The “U.S. Department of Energy (DoE)” has recommended criteria for hydrogen's adsorption energy and its gravimetric density in solid-state hydrogen storage materials. For optimal efficiency, the desired range for hydrogen's adsorption energy is -0.2 to -0.8 eV.[3] Furthermore, a convenient value for hydrogen's gravimetric density is 6.5 wt%. These criteria guide the selection of materials that allow for efficient hydrogen storage and help to build feasible solutions.[3]

As the first identified 2D material, graphene has paved the path for substantial research and exploration for additional 2D materials.[7] These materials, with their particular physical and chemical properties, have piqued the curiosity of researchers in a variety of fields. At cryogenic and ambient temperature, pristine graphene sheet is inefficient for hydrogen storage.[8] To improve hydrogen storage properties, several strategies such as metal atom doping, strain and defect generation have been intensively researched.[7,9-13] Yali and coworkers enhanced the hydrogen storage properties by decorating graphene with Ti metal, resulting in significant improvements in hydrogen storage capacity.[10] In addition, the integration of Ti atom into double vacancy defective graphene is regarded as an excellent method for storing hydrogen.[11] Furthermore, investigations have delved into the potential of Y doped graphene as a viable and reversible medium for hydrogen storage, exhibiting an impressive storage capacity of 6.17 wt%.[12] Additionally, the examination of Y decorated boron doped graphene has highlighted its potential as a medium for hydrogen storage.[13] Miao et al. investigated strain-engineered graphene with metal atom decorations for hydrogen storage. They discovered that 10% strain in a graphene enhanced the adsorption strength of Li (Ti) atoms by around 75% (71%), allowing them to attain hydrogen storage densities greater than the DoE's limit.[14] Likewise, a study employing molecular dynamic simulations demonstrated the potential of strained and defect-engineered graphene for hydrogen storage purpose.[15] Moreover, an allotrope of graphene known as 2D h-BN has garnered substantial attention for its diverse applications.[16] Investigations have revealed that in its pristine form, h-BN does not possess the necessary attributes for effective hydrogen storage. However, researchers discovered that by decorating Ti atom over C doped h-BN considerably improves hydrogen storage capacity.[17] Jing and collaborators studied expanded hexagonal boron nitride (eh-BN) for hydrogen storage. They found that the eh-BN could store up to 2.96 wt% hydrogen at 243K and 10MPa, falling short of the DoE's hydrogen storage standard.[18] Similarly, various methodologies, including the Ti

doped into divacancy h-BN, hydrogenated h-BN with Li functionality and decoration of Ni over defective h-BN, showcase substantial improvements in hydrogen storage properties when compared to the pristine configuration.[19-21] Furthermore, the work by Zhang and co-authors highlighted a significant improvement in hydrogen storage capacity, reaching 7.5 wt%, by incorporating Li doping into the structure of 2D porous boron nitride (p-BN).[22] Similarly, investigations have been conducted on B_6H_6 complexes decorated with alkaline earth, alkali and transition metals for storage of hydrogen, revealing excellent performance for hydrogen storage.[23]

Recently, Demirci et al. have predicted 2D orthorhombic diboron dinitride (o-B_2N_2) with exceptional thermal and dynamic stability.[24] This newly predicted 2D o-B_2N_2 has an orthorhombic lattice and semiconductor characteristics, with the band gap of 0.64 eV. The nature of this structure, which is made up of diatomic building blocks, suggests that 2D o-B_2N_2 might be synthesized utilizing precursor materials containing N-N and B-B bonds.[24] As described in introduction of Chapter 4, the 2D o-B_2N_2 material has been investigated for applications in the fields of optoelectronics, batteries, sensing and catalysis.[25-29]

Additionally, a study suggests Li decorated 2D o-B_2N_2 for hydrogen storage, showing remarkable 12.4 wt% capacity. This material holds promise for efficient lightweight hydrogen storage.[30] As per the literature survey, the hydrogen storage potential of pristine, defected and metals (Be, Mg, and Ca alkaline earth metals, Na and K alkali metals, as well as Y, Sc, Ti, and Zr transition metals) decorated 2D o-B_2N_2 has not been explored yet. This study is designed to assess the potential of these materials for hydrogen storage application.

5.2 Computational Details

In this chapter, the analysis of the hydrogen storage properties of the 2D o-B_2N_2 in its original form, with defects and under metals decoration were conducted using DFT

simulations. These calculations were performed using the Quantum ESPRESSO software.[31] The exchange-correlation interaction was treated using the Perdew-Burke-Ernzerhof (PBE) generalized gradient approximation (GGA).[32] The correction to the long-range interactions has been achieved by implementing the Grimme-D3 correction.[33] To accurately represent the 2D nature of the material, 30 Å vacuum was added perpendicular to the plane of the monolayer. This modification successfully eliminated any interactions between the periodic images, ensuring an accurate simulation. The electronic wave functions were expanded using the plane wave basis set with the cut-off energies 70 Ry for the wave functions. The integration of the Brillouin zone was carried out using the Monkhorst-Pack scheme on 5×10×1 *k*-point mesh.[34] To obtain the relaxed configuration for each considered structure, an iterative convergence process was employed until the maximum Hellmann-Feynman force acting on each atom reached a value lower than 10^{-3} eV/Å.

5.3 Results and Discussion

5.3.1 Pristine 2D o-B_2N_2

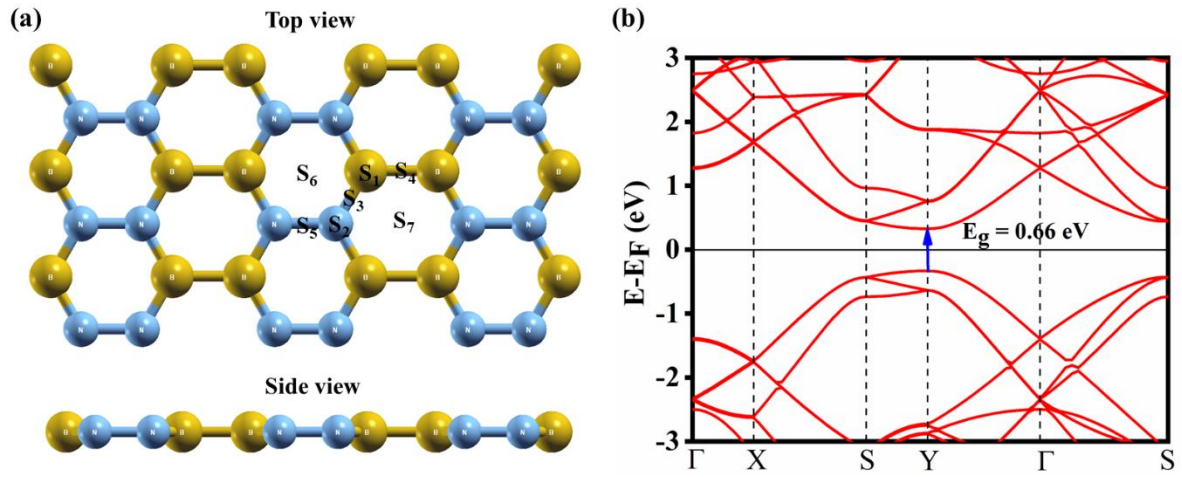

Figure 5.1: The structural geometry (a) and band structure (b) of the 2D o-B_2N_2.

To check the hydrogen storage properties of the 2D o-B_2N_2, we optimized a supercell with dimensions of 3×3×1. Fig. 5.1(a and b) depicts the structural geometry and band structure of the 2D o-B_2N_2. The lattice parameters a and b of the 2D o-B_2N_2 with a size of 3×3×1 is 13.65

Å and 7.44 Å, respectively. The obtained bond lengths for B-B, N-N and B-N are 1.69 Å, 1.43 Å and 1.43 Å, respectively (see Fig. 5.1(a)). Additionally, the band gap is determined to be 0.66 eV (see Fig. 5.1(b)). These findings demonstrate a significant alignment with results reported in earlier studies.[24-26,29,30]

To check the potential of 2D o-B_2N_2 for hydrogen storage, we initially adsorbed hydrogen molecule onto all the designated sites (S_1 to S_7) of the pristine monolayer (refer to Fig. 5.1(a)). We have calculated the adsorption energy (E_{ad})[19,22,30] of the first hydrogen using following equation:

$$E_{ad} = E(H_2 + Monolayer) - E(Monolayer) - E(H_2) \text{ -----(5.1).}$$

Where, E(H_2+Monolayer) represents the total energy of the hydrogen adsorbed monolayer, E(Monolayer) represents the total energy of the considered monolayer and E(H_2) represents the total energy of the isolated hydrogen molecule. Using equation (5.1), the determined E_{ad} values for all locations are below -0.06 eV, as detailed in Table 5.1. These results fall outside the range outlined in the guidelines by the DoE. As a result, it can be inferred that the unmodified 2D o-B_2N_2 is unsuitable for application as a hydrogen storage material.

Table 5.1: The adsorption energy of the first hydrogen molecule over 2D o-B_2N_2.

Sites	**S_1**	**S_2**	**S_3**	**S_4**	**S_5**	**S_6**	**S_7**
E_{ad} (eV)	-0.05	-0.06	-0.06	-0.05	-0.06	-0.05	-0.05

5.3.2 Alkali and Alkaline-Earth Metals Decorated 2D o-B_2N_2

As stated in the introduction, Li decorated 2D o-B_2N_2 has been investigated as an effective hydrogen storage medium with a remarkable capacity for hydrogen storage of 12.4 wt%.[30] In a recent study, Mahamiya and colleagues proved that the original 4-6-8 biphenylene sheet doesn't effectively store hydrogen. Nonetheless, the hydrogen storage characteristics exhibit notable enhancement through the introduction of alkali metals like Na and K, along

with alkaline-earth metals such as Be, Mg, and Ca.[35] According to the literature survey, the hydrogen storage capability of metal decorated 2D o-B_2N_2 has not explored. This section concentrated on these specific cases. To check the binding of metals to the 2D o-B_2N_2, we first decorated metals (see Fig. 5.1(a)) at all available sites (S_1 to S_7) and estimated the binding energy (E_b)[35-37] using following equation:

$$E_b = \frac{E(\text{Metals + Monolayer}) - E(\text{Monolayer}) - n \times E(\text{Metal})}{n} \text{ -----(5.2).}$$

Where, E(Metals + Monolayer) represents the total energy of the metals decorated 2D o-B_2N_2, E(Metal) represents the total energy of the isolated metals and n represents total number of the decorated metals.

Table 5.2: Binding energy of Na, K, Be, Mg and Ca metals at possible sites of the 2D o-B_2N_2, respectively.

Initial Site	Na		K		Be		Mg		Ca	
	Final Site	E_b (eV)	Final Site	E_b (eV)	Final Site	E_b (eV)	Final Site	E_b (eV)	Final Site	E_b (eV)
S_1	S_7	-0.77	S_1	-0.98	S_4	-0.38	S_4	-0.33	S_7	-0.69
S_2	S_2	-0.59	S_6	-1.10	S_4	-0.38	S_2	-0.25	S_5	-0.55
S_3	S_7	-0.77	S_6	-1.10	S_4	-0.38	S_4	-0.33	S_7	-0.69
S_4	S_4	-0.62	S_4	-1.00	S_4	**-0.38**	S_4	**-0.33**	S_4	-0.54
S_5	S_5	-0.61	S_5	-1.01	S_5	-0.18	S_5	-0.25	S_5	-0.55
S_6	S_6	-0.64	S_6	**-1.10**	S_6	-0.21	S_6	-0.27	S_6	-0.57
S_7	S_7	**-0.77**	S_7	-1.09	S_4	-0.38	S_7	-0.29	S_7	**-0.69**

The computed E_b values (using equation (5.2)) for all scenarios, encompassing both the initial and concluding positions, have been listed in Table 5.2. For the decoration of the metals Na, K, Be, Mg and Ca, the sites S_7, S_6, S_4, S_4 and S_7 are found to exhibit the minimum energy configurations, respectively (see Table 5.2). The structural geometries for these sites are depicted in Fig. 5.2. The calculated E_b is -0.77 eV, -1.10 eV, -0.38 eV, -0.33 eV and -0.69 eV for Na, K, Be, Mg and Ca metals, respectively. For Na, Be, Mg and Ca metals decoration cases,

E_b is lower than the cohesive energy of the respective bulk.[35] Consequently, there is a high chance of cluster formation. However, when considering K adsorption, E_b is higher than the cohesive energy of bulk K (0.93 eV), making it a potentially excellent medium for hydrogen storage.[35]

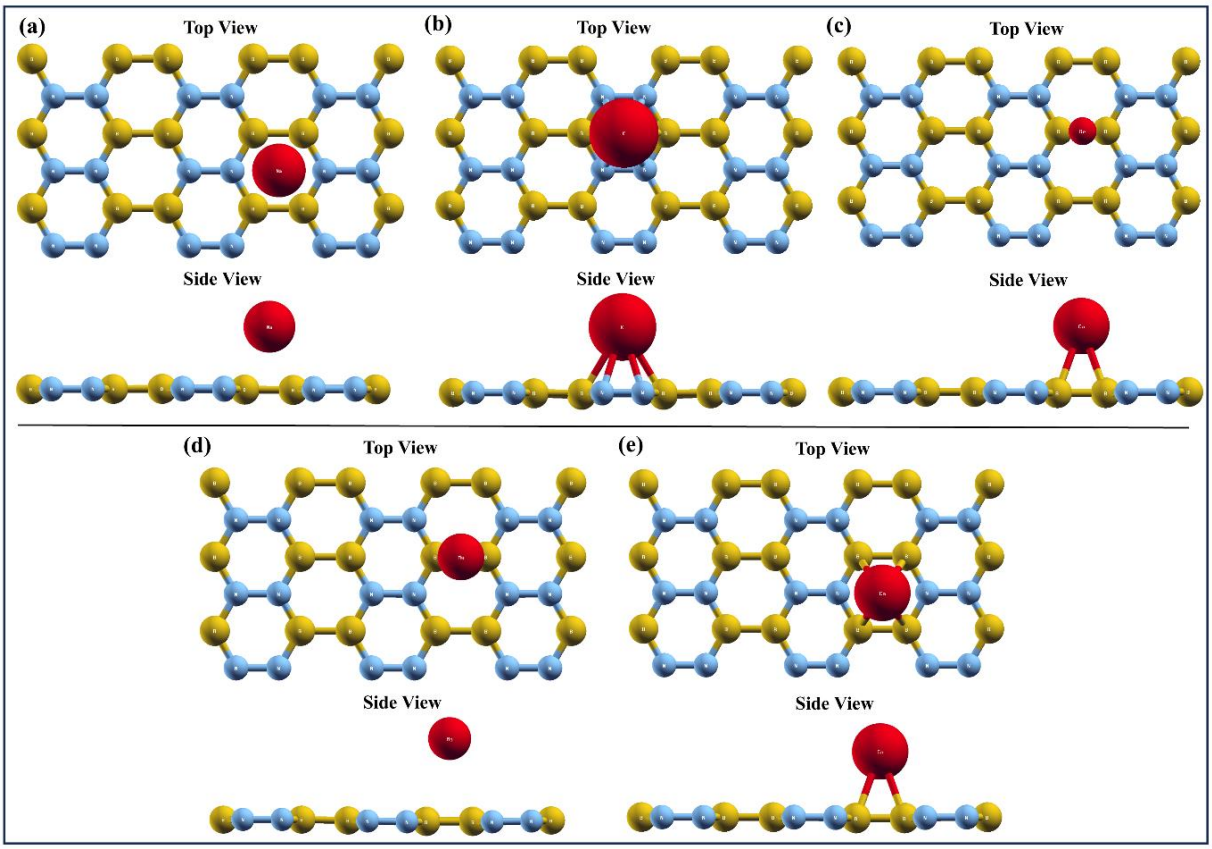

Figure 5.2: The structural geometry of the Na (a), K (b), Be (c), Mg (d) and Ca (e) decorated 2D o-B_2N_2, respectively.

To assess the E_{ad} of hydrogen across all five aforementioned scenarios, we initiated the process by introducing a hydrogen molecule for adsorption onto each metals decorated 2D o-B_2N_2. The computed E_{ad} values for the first hydrogen molecule (calculated using equation (5.1)) are as follows: -0.006 eV for Na decoration, -0.01 eV for K decoration, -0.02 eV for Be decoration, -0.03 eV for Mg decoration and -0.02 eV for Ca decoration on the 2D o-B_2N_2. These outcomes collectively indicate that the utilization of mentioned metals decorated 2D o-B_2N_2 is unsuitable as a substrate for hydrogen storage.

5.3.3 Defected 2D o-B_2N_2

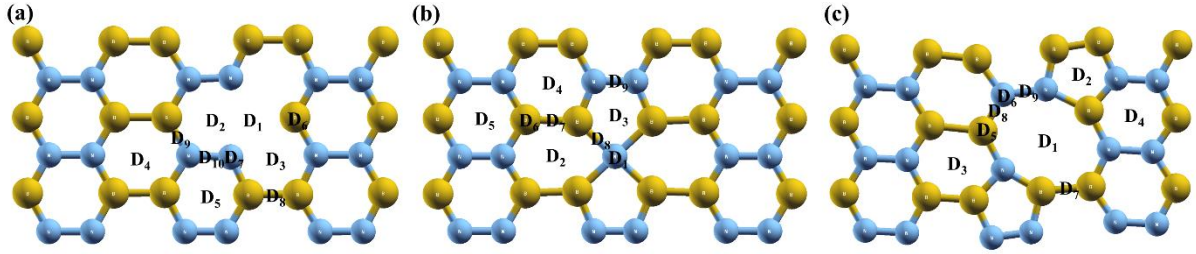

Figure 5.3: The structural geometry of the B (a), N (b) and BN (c) defected 2D o-B_2N_2, respectively.

Table 5.3: The adsorption energy of the first hydrogen molecule on various sites of B, N, and BN defected 2D o-B_2N_2, respectively.

B defect		N defect		BN defect	
Sites	**E_{ad} (eV)**	**Sites**	**E_{ad} (eV)**	**Sites**	**E_{ad} (eV)**
D_1	-0.11	**D_1**	-0.05	**D_1**	-0.06
D_2	-0.11	**D_2**	-0.06	**D_2**	-0.07
D_3	-0.10	**D_3**	-0.06	**D_3**	-0.06
D_4	-0.09	**D_4**	-0.06	**D_4**	-0.07
D_5	-0.11	**D_5**	-0.06	**D_5**	-0.05
D_6	-0.07	**D_6**	-0.06	**D_6**	-0.06
D_7	-0.11	**D_7**	-0.06	**D_7**	-0.06
D_8	-0.09	**D_8**	-0.05	**D_8**	-0.05
D_9	-0.08	**D_9**	-0.06	**D_9**	-0.06
D_{10}	-0.10				

In previous Chapter, we assessed the HER performance of 2D o-B_2N_2 with B, N and BN defects. The stability of these defected monolayers was verified via formation energy and AIMD simulations at 300 K. However, the potential of defective monolayers for hydrogen storage has not been investigated. In this study, we concentrate on uncovering the hydrogen storage suitability of these defected monolayers. Fig. 5.3 illustrates the structural geometry of these defective monolayers. For hydrogen storage assessment, we initially adsorbed hydrogen molecule at various potential sites, as depicted in Fig. 5.3. The calculated E_{ad} values, obtained

through equation (5.1), are compiled in Table 5.3. These E_{ad} values for defected monolayers are below -0.12 eV, failing to meet the DoE criteria. Consequently, just like pristine and metals (Na, K, Be, Mg, and Ca) decorated 2D o-B_2N_2, defected monolayers are also unsuitable for hydrogen storage.

5.3.4 Transition Metals Decorated 2D o-B_2N_2

5.3.4.1 Interaction of Transition Metals with 2D o-B_2N_2

Table 5.4: Binding energy of Sc, Ti, Y and Zr metals at all possible sites of the 2D o-B_2N_2, respectively.

Initial Site	Sc		Ti		Y		Zr	
	Final Site	E_b (eV)	Final Site	E_b (eV)	Final Site	E_b (eV)	Final Site	E_b (eV)
S_1	S_1	-2.37	S_1	-2.44	S_4	-2.21	S_1	-1.98
S_2	S_2	-1.90	S_2	-2.49	S_7	-2.23	S_2	-2.13
S_3	S_7	-2.55	S_7	-2.79	S_7	-2.24	S_6	-2.19
S_4	S_4	-2.37	S_7	-2.77	S_4	-2.21	S_4	**-2.34**
S_5	S_5	-1.94	S_5	-2.42	S_5	-1.80	S_5	-2.12
S_6	S_6	-2.25	S_6	-2.63	S_6	-1.93	S_6	-2.19
S_7	S_7	**-2.55**	S_7	**-2.79**	S_7	**-2.24**	S_4	-2.34

Based on the existing research, it has been found that enhancing the hydrogen storage properties of monolayers can be achieved by decorating them with transition metals like Sc, Ti, Y and Zr.[7,10,12,38] Inspired by these discoveries, our study focused on incorporating these metals onto different feasible sites (refer to Fig. 5.1(a)). Then, we used equation (5.2) to calculate E_b and the results are presented in Table 5.4. Among the various sites considered, the S_7 site exhibited the lowest energy for Sc, Ti and Y metals, while the S_4 site showed the lowest energy for Zr metal. The structural configurations are visualized in Fig. 5.4. Notably, for the cases with the lowest energy, the calculated E_b values were -2.55 eV, -2.79 eV, -2.24 eV and

-2.34 eV for Sc, Ti, Y and Zr metals decoration, respectively. These values indicate a strong interaction between them.

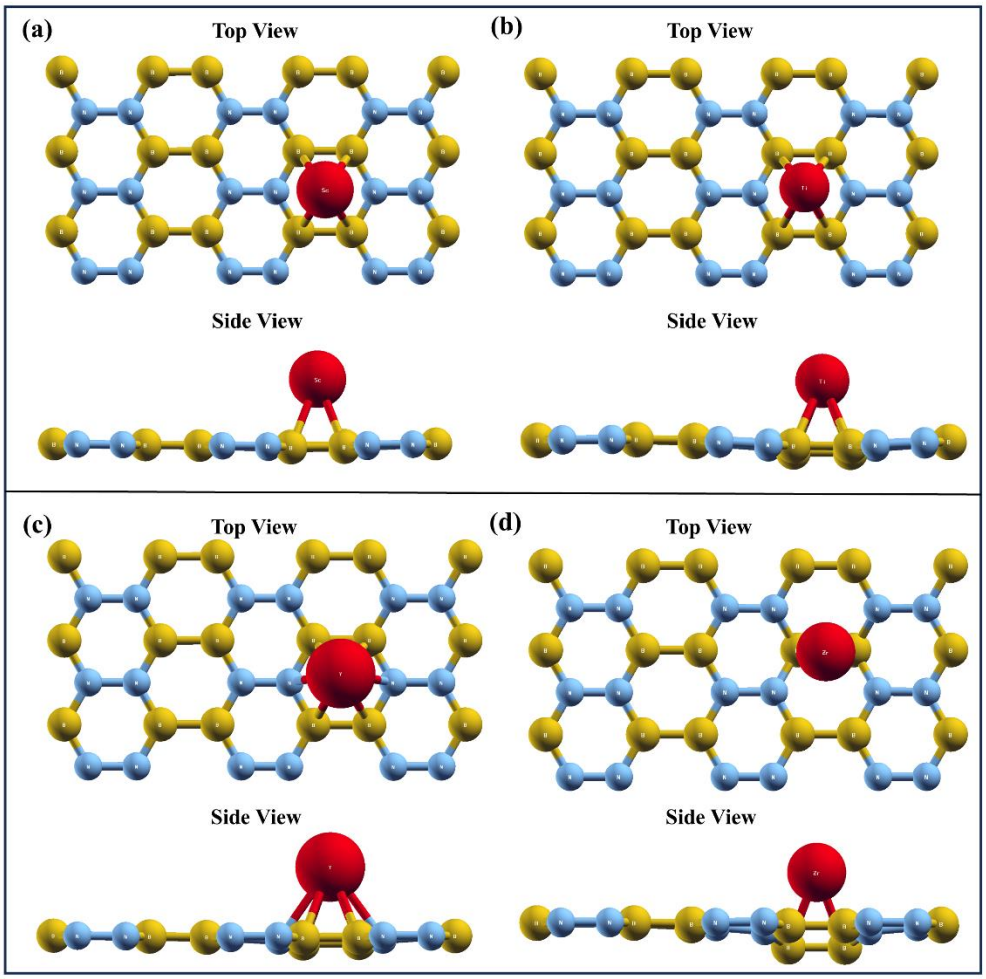

Figure 5.4: The optimized geometry of the Sc (a), Ti (b), Y (c) and Zr (e) decorated 2D o-B_2N_2, respectively.

In the present cases, the average distances from the metals (Sc, Ti and Y) to the B atom are 2.61 Å, 2.48 Å and 2.66 Å, respectively. In the case of the Zr atom, the average distance from the Zr metal to the N atoms is 2.34 Å. The average B-B (B-N) bond become 1.66 Å (1.44 Å), 1.65 Å (1.45 Å) and 1.65 Å (1.45 Å) from 1.69 Å (1.43 Å) for the Sc, Ti and Y decoration cases, respectively. For Zr decoration, the N-N bond becomes 1.48 Å from 1.43 Å. These observed alterations in the structural parameters can be ascribed to the substantial interaction

occurring between the 2D o-B_2N_2 and the considered metals, which further validating the calculated E_b values.

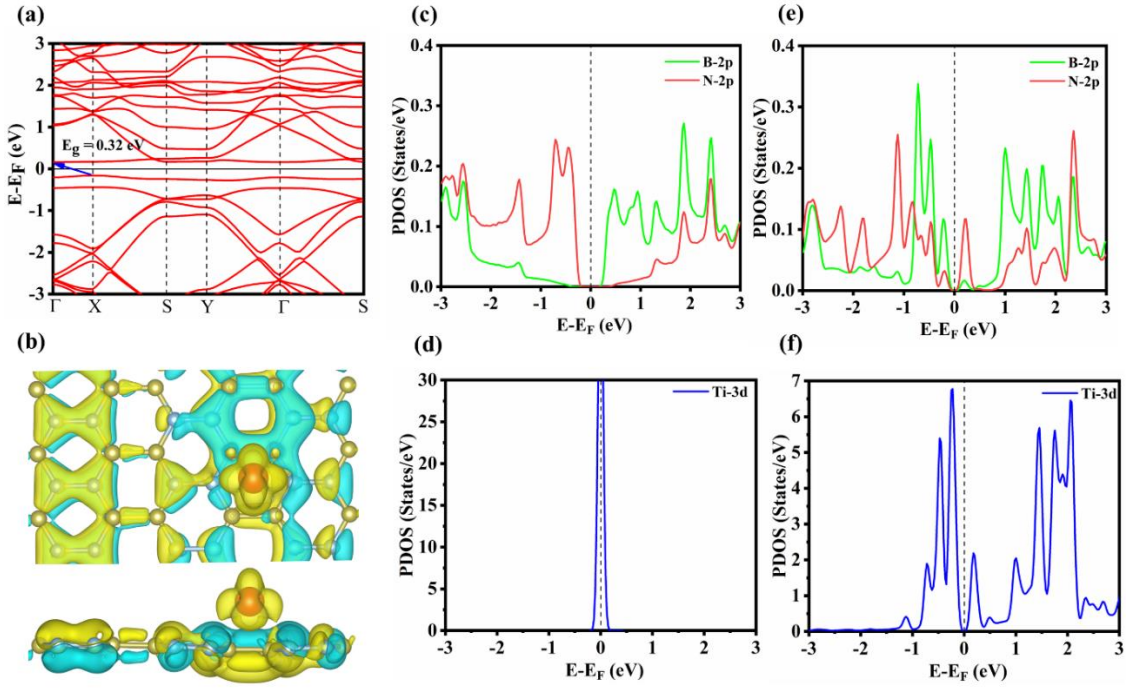

Figure 5.5: Band structure (a), charge density difference plot (b) and PDOS (e and f) of Ti decorated 2D o-B_2N_2; PDOS of the pristine 2D o-B_2N_2 (c) and isolated Ti atom (d), respectively.

5.3.4.2 Adsorption of the First Hydrogen Molecule over Transition Metals Decorated 2D o-B_2N_2

To study the hydrogen storage properties of 2D o-B_2N_2 with transition metals decoration, we began by adsorbing the first hydrogen molecule. Utilizing equation (5.1), the obtained E_{ad} for the first hydrogen molecule is -0.01 eV, -0.47 eV, -0.01 eV and -0.04 eV for Sc, Ti, Y and Zr decoration cases, respectively. In the context of Sc, Y and Zr decoration scenarios, it was noted that the hydrogen molecule positioned itself at distances of 3.45 Å, 4.20 Å and 3.13 Å from the transition metal sites, respectively. Interestingly, these distances did not result in any alteration in the bond length of hydrogen molecule. The convergence of factors such as negligible E_{ad}, considerable adsorption separation and the consistent preservation of the hydrogen molecule's bond length implies that the viability of Sc, Y and Zr decoration cases

for hydrogen storage has been ruled out. In the case of the Ti decoration case, it was observed that the hydrogen molecule positioned itself at a distance of 1.91 Å from the Ti metal. This resulted in an elongation of the bond length, stretching it from 0.74 Å to 0.89 Å. The alignment of the E_{ad} value with the DoE criteria, along with the close adsorption distance and elongated hydrogen bond length, highlights the system's potential as a promising candidate for hydrogen storage. Using these findings as a guide, we will only look into studying the electronic properties and hydrogen molecules adsorption on the Ti decorated 2D o-B_2N_2.

5.3.4.3 Electronic Properties of the Ti decorated 2D o-B_2N_2

Fig. 5.5(a) illustrates the band structure of Ti decorated 2D o-B_2N_2. The incorporation of Ti leads to a reduction in the band gap of the 2D o-B_2N_2, decreasing it from 0.66 eV to 0.32 eV. This significant decrease in the band gap serves as a compelling indication of the increased conductivity. Fig. 5.5(c and d) displays the PDOS for the pristine 2D o-B_2N_2 and an individual isolated Ti atom, respectively. Meanwhile, Fig. 5.5(e and f) depicts the p orbitals of B and N atoms, as well as the Ti-3d orbitals, within the 2D o-B_2N_2 decorated with Ti. After Ti decoration, we clearly observed an enhancement in p orbitals of the B and N atoms near E_F (see Fig. 5.5(e)) as compared to the bare 2D o-B_2N_2 (see Fig. 5.5(c)), respectively. Simultaneously, a decrement in the intensity of the d orbitals of Ti is observed (see Fig. 5.5(f)) at E_F as compared to d orbitals of the isolated Ti atom (see Fig. 5.5(d)). This observation suggests that charge donation from the Ti atom to the 2D o-B_2N_2, as indicated by the enhancement in the p orbitals of B and N atoms and the reduction in the Ti-3d orbitals at the E_F. After the Ti decoration, the Löwdin charge analysis revealed that the average charges over the B atoms (N atoms) changed from 5.1367*e* (2.8439*e*) to 5.1518*e* (2.8747*e*), while the charges over the Ti atom changed from 3.9988*e* (charge of isolated Ti atom) to 3.1790*e*. This indicates a clear charge donation from the Ti atom to the 2D o-B_2N_2 and is accordance with the charge transfer analysis from the PDOS. Furthermore, we have also plotted the CDD between the Ti

decorated 2D o-B_2N_2 and the pristine 2D o-B_2N_2 (see Fig. 5.5(b)) to confirm the above charge transfer analysis. In this plot, the cyan colour indicates charge accumulation, while the yellow colour represents the charge depletion layer. Here, we also observe the charge depletion layer over the Ti, confirming that Ti loses charge to the 2D o-B_2N_2.

5.3.4.4 Electronic Properties of the First Hydrogen Molecule Adsorbed Ti Decorated 2D o-B_2N_2

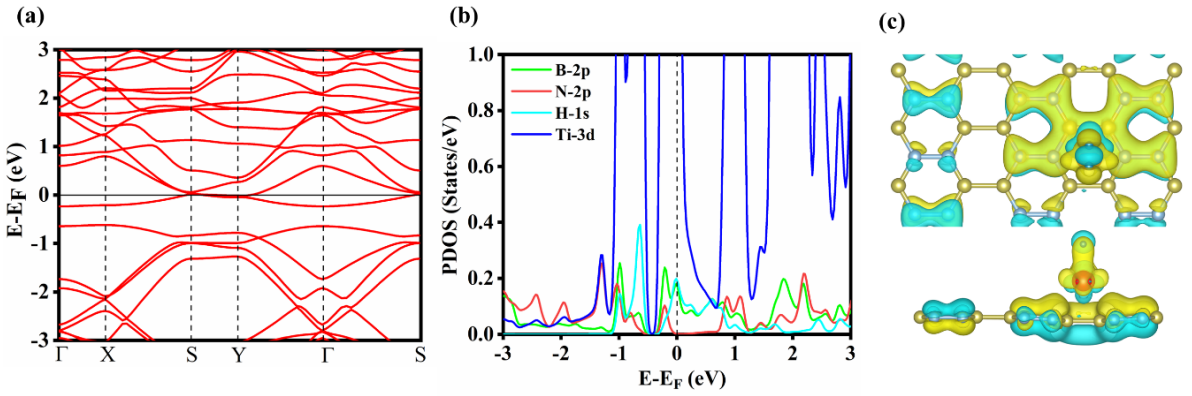

Figure 5.6: Band structure (a), PDOS (b) and charge density difference plot (c) of the hydrogen molecule adsorbed over Ti decorated 2D o-B_2N_2, respectively.

Fig. 5.6(a and b) illustrates the band structure and PDOS corresponding to the hydrogen adsorption on Ti decorated 2D o-B_2N_2. These plots depict the transformation to a metallic behaviour upon the introduction of hydrogen molecule through adsorption. From the PDOS (refer to Fig. 5.6(b)), it is evident that the H-1s orbitals divided into VBM and CBM, confirming its adsorption. The metallic characteristics are attributed to the presence of Ti-3d, H-1s and B-2p orbitals, while an overlap between these distinct orbitals signifies hybridization among them. After hydrogen adsorption, the Löwdin charge analysis revealed that the average charges over the B atoms (N atoms) changed to 5.1484*e* (2.8691*e*) from 5.1518*e* (2.8747*e*), while the charges over the Ti atom changed to 3.2188*e* from 3.1790*e*. Simultaneously, an observed total charge gain of 0.1571e occurs on the hydrogen molecule. Charge transfer results show that charge donation towards the Ti metal and hydrogen molecule from the monolayer is noted. In addition, we plotted the CDD among hydrogen molecule adsorbed over the Ti decorated 2D o-

B_2N_2, the Ti decorated 2D o-B_2N_2 itself and the isolated hydrogen molecule (refer to Fig. 5.6(c)) to confirm charge analysis. In this plot, the cyan colour indicates charge accumulation, while the yellow colour represents the charge depletion layer. Importantly, we noticed a decrease in charge around the adsorbed area of monolayer, while there was a noticeable increase in charge around the Ti metal and hydrogen molecule. It's worth mentioning that the outcomes from both Löwdin charge transfer and CDD plot align with each other.

Table 5.5: Adsorption energy of the hydrogen molecules over one and two Ti decorated 2D o-B_2N_2, respectively.

Ti/o-B_2N_2		**2Ti/o-B_2N_2**	
Number of H_2	**E_{ad} (eV/H_2)**	**Number of H_2**	**E_{ad} (eV/H_2)**
1H_2	-0.47	**6H_2**	-0.66
2H_2	-0.80	**8H_2**	-0.59
3H_2	-0.69	**10H_2**	-0.52
4H_2	-0.60	**18H_2**	-0.31
5H_2	-0.48	**26H_2**	-0.23
6H_2	-0.41	**27H_2**	-0.23
7H_2	-0.36	**28H_2**	-0.22
8H_2	-0.32	**29H_2**	-0.22
9H_2	-0.29	**30H_2**	-0.21
10H_2	-0.26	**31H_2**	-0.21
11H_2	-0.24	**32H_2**	-0.21
12H_2	-0.23	**33H_2**	-0.20
13H_2	-0.21	**34H_2**	-0.20
14H_2	-0.20	**35H_2**	-0.19
15H_2	-0.19	**36H_2**	-0.19

5.3.4.5 Adsorption of the Hydrogen Molecules over Ti decorated 2D o-B_2N_2

The gravimetric storage capacity (G_{SC}) is vital for hydrogen storage usability. For G_{SC} calculation, we adsorbed hydrogen molecules one by one up to a total of fifteen molecules on

Ti decorated 2D o-B_2N_2, respectively. The average E_{ad} per molecule is calculated using following equation[39]:

$$E_{ad} = \frac{E(nH_2 + \text{Monolayer}) - E(\text{Monolayer}) - n \times E(H_2)}{n} \text{-----(5.3).}$$

Here, n is total number of adsorbed the hydrogen molecule.

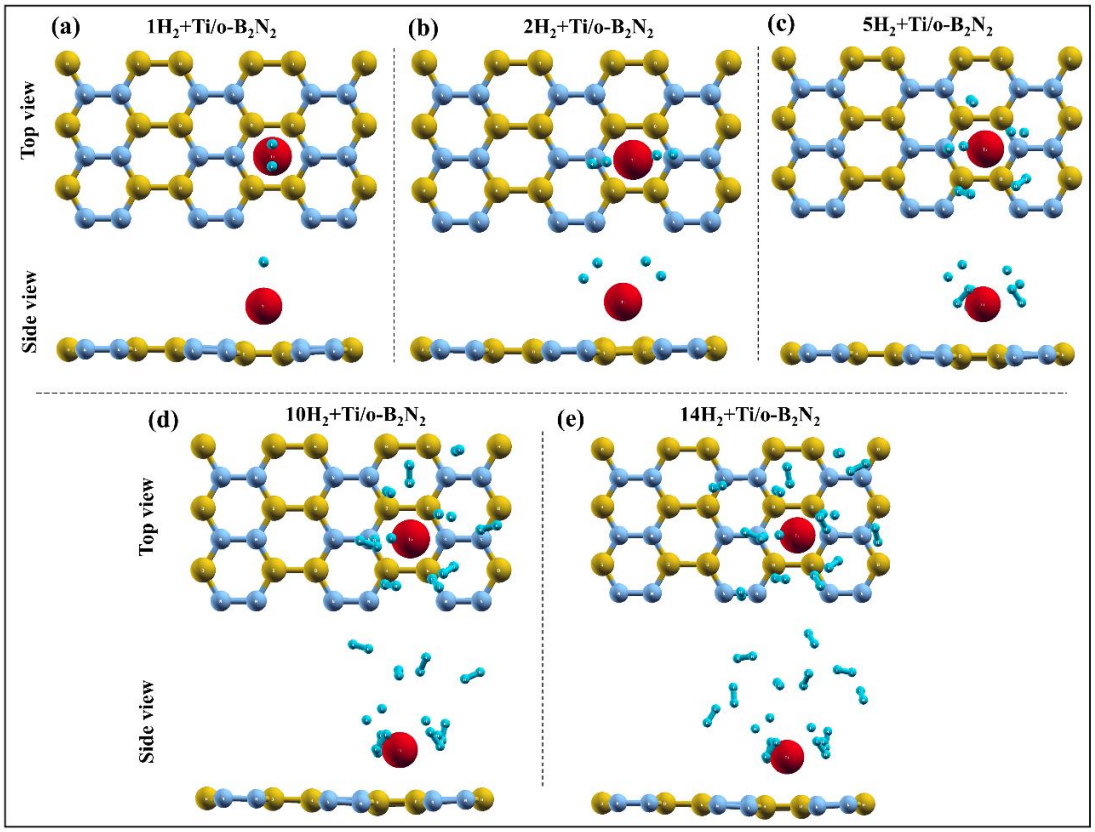

Figure 5.7: The structural geometry of one (a), two (b), five (c), ten (d) and fourteen (e) hydrogen molecules adsorbed Ti decorated 2D o-B_2N_2, respectively.

The calculated average E_{ad} values, obtained using equation (5.3), are given in Table 5.5. Up to the adsorption of fourteen hydrogen molecules, the calculated E_{ad} values are within the DoE criteria. However, with the adsorption of the fifteenth hydrogen molecule, the average E_{ad} falls beyond the DoE's prescribed range. Specifically, the average E_{ad} for the adsorption of fourteen hydrogen molecules onto Ti decorated 2D o-B_2N_2 stands at -0.39 eV/H_2. The Fig. 5.7 displays the structural representation of the one, two, five, ten and fourteen hydrogen molecules adsorbed Ti decorated 2D o-B_2N_2, respectively. In the hydrogen adsorbed Ti decorated 2D o-

B_2N_2, the bond length of the first five hydrogen molecules become 0.82 Å, 0.82 Å, 0.82 Å, 0.78 Å and 0.78 Å from 0.74 Å, respectively (see Fig. 5.7(c)). Here, average H-H bonds are longer than bond length of free hydrogen molecule, indicating a stronger interaction than physisorption. Furthermore, this elongation in the hydrogen molecules bond length suggests that Kubas-type interactions play a role in the considered system. In these interactions, there is charge donation from the metal towards the adsorbed hydrogen and back-donation from hydrogen towards the metal, resulting in the enhancing of H-H bond length.[40,41]

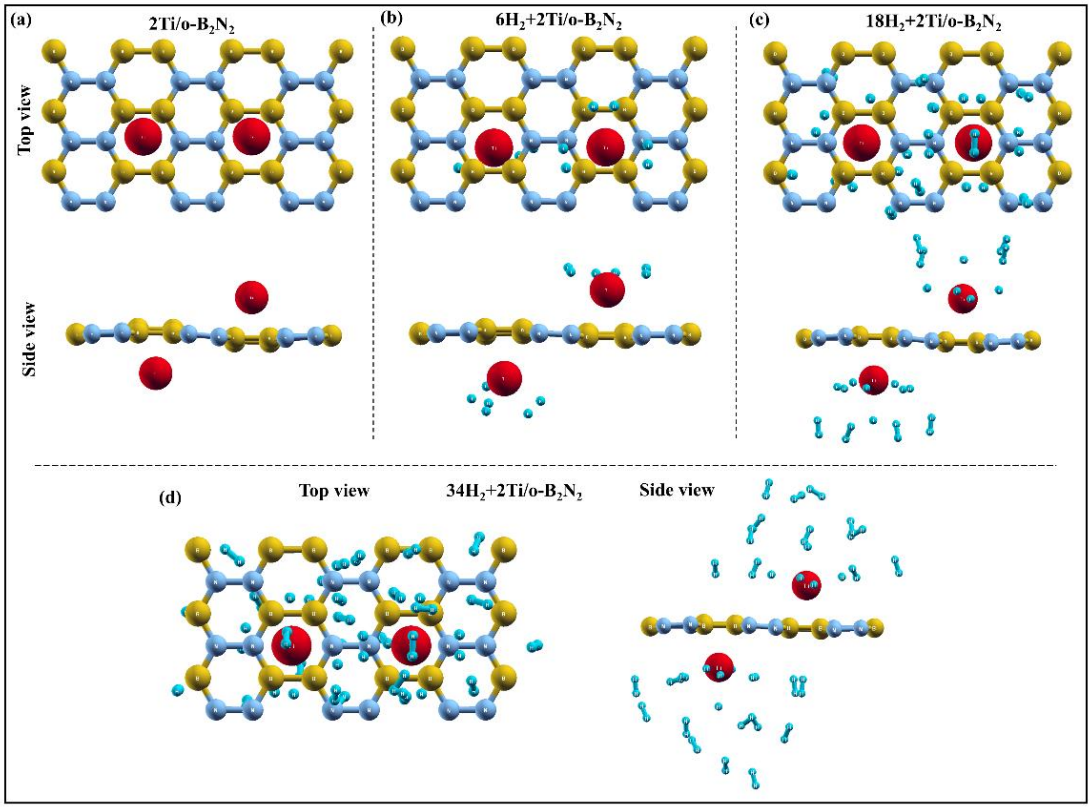

Figure 5.8: The structural geometry of two Ti decorated 2D o-B_2N_2 (a); and six (b), eighteen (c) and thirty-four (d) hydrogen molecules adsorbed on two Ti decorated 2D o-B_2N_2, respectively.

A review of the literature indicates the feasibility of decorating transition metals on both sides of the 2D systems.[39-41] In this study, we have decorated a second Ti atom at three distinct sites: adjacent to the neighbouring S_7 site, on the same site but situated on the monolayer's opposite side and at the diagonally opposite side, respectively. Among these, the second Ti atom is anchored to the diagonally opposite side of the monolayer, exhibiting the E_b of -2.81

eV, all the while retaining its initial adsorption site intact. Fig. 5.8(a) depicts structural geometry for the two Ti decorated 2D o-B_2N_2, respectively. Furthermore, to obtain the G_{SC}, we have adsorbed and calculated average E_{ad} up to thirty-six hydrogen molecules over two Ti decorated 2D o-B_2N_2, respectively. As presented in Table 5.5, the E_{ad} values for thirty-four hydrogen molecules are within the limits specified by DoE range. However, for thirty-five and thirty-six hydrogen molecules, the average E_{ad} values fall outside the DoE limits. As conclusion, we can conclude that the two Ti decorated 2D o-B_2N_2 can bind a total of thirty-four hydrogen molecules, with average E_{ad} of -0.31 eV/H_2.

5.3.4.6 Gravimetric Storage Capacity for Hydrogen Storage and Desorption Temperature Calculation

The G_{SC} is calculated by following equation[39]:

$$G_{SC}\,(wt\%) = \frac{n_{H_2} \times w_{H_2}}{n_B \times w_B + n_N \times w_N + n_{Ti} \times w_{Ti} + n_{H_2} \times w_{H_2}} \text{ -----(5.4).}$$

Here, n_{H_2}, n_B , n_N and n_{Ti} are total number of hydrogen molecules, B atoms, N atoms and Ti atoms, respectively and w_B , w_N , w_{Ti} and w_{H_2} are the total weight of the B atoms, N atoms, Ti atoms and hydrogen molecules, respectively. Here, we have considered a 3x3x1 supercell of the 2D o-B_2N_2, which contains a total of eighteen B atoms and eighteen N atoms, respectively. Additionally, we adsorbed thirty-four hydrogen molecules on two Ti decorated 2D o-B_2N_2. Using the above information and equation (5.4), the derived G_{SC} (wt%) is 11.21%.

The "desorption temperature" (T_D)[38] of the hydrogen adsorbed system plays a crucial role for practical application. We have calculated T_D using the "van't Hoff equation", as given below:

$$T_D = \frac{E_{ad}}{k_b} \times \left(\frac{\Delta S}{R}\right)^{-1} \text{ -----(5.5).}$$

Where, "k_b is Boltzmann constant (1.380×10^{-23} J K^{-1}), ΔS is change of hydrogen entropy from gas to liquid phase (75.44 J mol^{-1} K^{-1}) and R is universal gas constant (8.314 J mol^{-1} K^{-1})". Using equation (5.5), the obtained T_D is ~ 396 K.

5.3.4.7 Stability Assessment at Desorption Temperature from AIMD Calculation

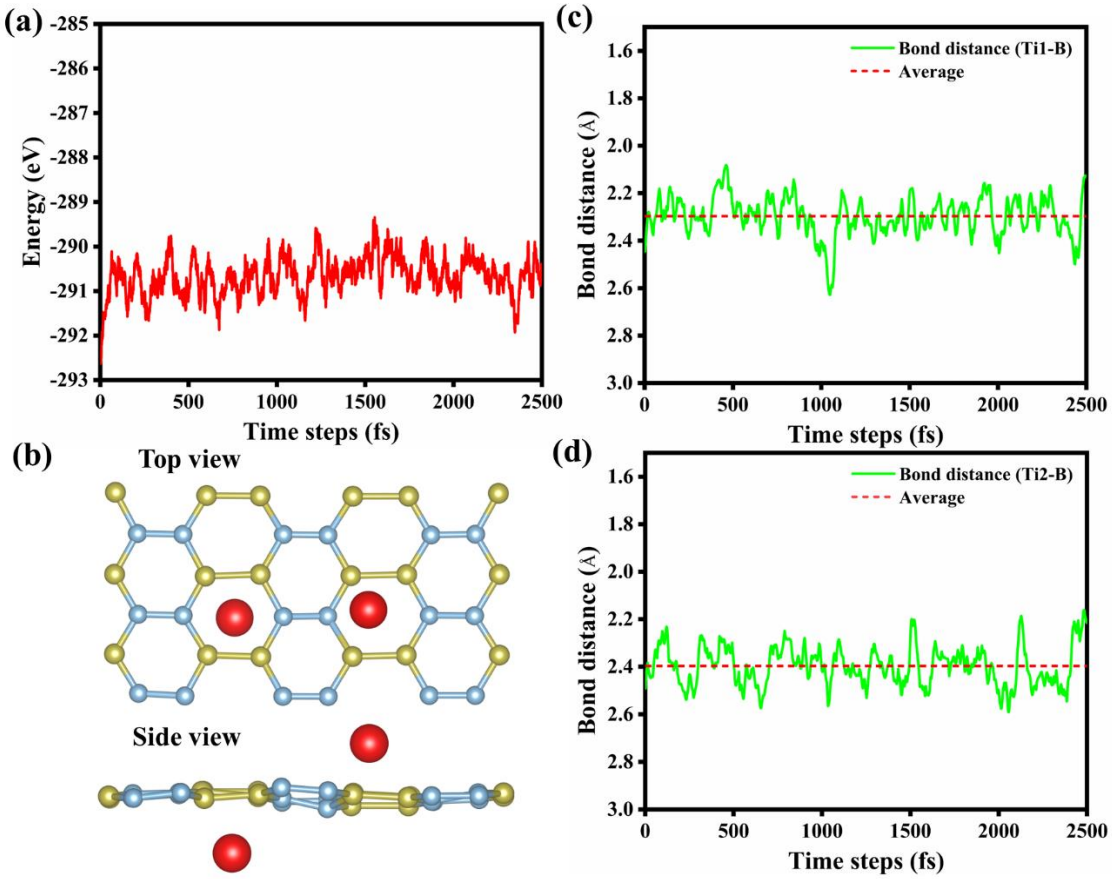

Figure 5.9: The results of AIMD simulation: The energy vs time step plot (a), top and side view of structural geometry (b) and variation in bond distances (Ti1-B (c) and Ti2-B (d)) plots of 2Ti/o-B_2N_2 at 396 K, respectively.

The material must be capable of retaining its stability at T_D to be a viable candidate for hydrogen uptake. To assess this, AIMD simulations were conducted on two Ti decorated 2D o-B_2N_2 at 396 K, using the NVT ensemble within the VASP package. The simulation results, displayed in Fig. 5.9, demonstrate the binding of the two Ti onto the 2D o-B_2N_2. The energy values exhibit fluctuations around the mean value, indicating that the two Ti decorated 2D o-B_2N_2 remains stable at 396 K (see Fig. 5.9(a)). In simple term, considered system does not break or distorted at 396 K, signifying that the system maintains its thermal stability (Fig.

5.9(b)). This observation confirms that the material is a suitable and convenient choice for hydrogen uptake application.

In addition, we have also plotted the changes/variations in bond distances between the Ti1 and B atoms, as well as between the Ti2 and B atoms. In Fig. 5.9(c and d), the thermal fluctuation in the bond distances of Ti1-B and Ti2-B over time are shown, indicating that the variations are not significantly high. These observations reveal the vibrational movement of the Ti atoms around its mean position only. Based on our findings, the Ti atom demonstrates remarkable integrity on the 2D o-B_2N_2 even at the higher temperature of 396 K, with minor bond distance changes. As a result, empirical evidence suggests that Ti decorated 2D o-B_2N_2 as hydrogen storage medium is feasible in practice.

Table 5.6: The comparison of the average adsorption energy per hydrogen molecule and gravimetric storage capacity of Ti decorated 2D o-B_2N_2 with various reported work.

System	E_{ad} (eV/H_2)	G_{sc} (wt%)	References
Ti decorated 2D o-B_2N_2	-0.31	11.21	Present work
Zr decorated psi-graphene	-0.38	11.3	7
Strained graphene	-0.42	9.40	9
Y decorated graphene	-0.568	5.78	13
eh-BN	-	2.96	18
Li doped p-BN	0.16	7.50	22
Li decorated o-B_2N_2	-0.22	12.40	30
K decorated biphenylene	-0.24	11.90	35
Ca decorated biphenylene	-0.33	11.63	35
Y decorated BeN_4	-0.38	10.11	36
Li decorated T-BN	0.245– 0.315	12.31	39
V decorated biphenylene	-0.51	7.52	40
Pure h-BN	0.128	6.70	42
Ni doped h-BN	-	7.30	43
Ti decorated HGY	-0.38	10.52	44
Ti decorated BNNT	-0.20	8.00	45

5.3.5 Drawing Comparison with Previous Studies

Here, we have compared the average E_{ad} and G_{SC} of our study with previous reports on hydrogen storage.[7,9,13,18,22,30,35,36,39,40,42-45] Detailed insights into this comparison are tabulated in Table 5.6. In addition, Table 5.6 signify that Ti decorated 2D o-B_2N_2 exhibits a superior G_{SC} compared to strained graphene, Y decorated graphene, eh-BN, Li doped p-BN, Y decorated BeN_4, pure h-BN, Ni doped h-BN, V decorated BeN_4 and Ti decorated BNNT. It also shows comparable performance to Zr decorated psi-graphene, Li decorated o-B_2N_2, K and Ca decorated biphenylene, Li decorated T-BN and Ti decorated holey graphyne. In summary, our theoretical study highlights the potential of Ti decorated 2D o-B_2N_2 as excellent hydrogen storage media, offering reliable stability at thermodynamic conditions and fulfilling the criteria set by DoE.

5.4 Conclusions

In summary, we conducted a study to explore the possibility of the pristine, defected and metals (including Na and K alkali metals, Be, Mg and Ca alkaline-earth metals and Sc, Ti, Y and Zr transition metals) decorated 2D o-B_2N_2 as a hydrogen storage medium through DFT calculations. The outcomes indicate that the pristine, defected and metals Na, K, Be, Mg, Ca, Sc, Y and Zr decorated 2D o-B_2N_2 did not align favourably with the DoE requirements for an effective hydrogen storage medium. Nonetheless, promising results emerged from the Ti decorated 2D o-B_2N_2, suggesting its suitability as a hydrogen storage medium. Notably, the Ti atoms exhibited a strong and favourable bonding with the 2D o-B_2N_2, leading to a decrement in the band gap and an increase in conductivity. The E_{ad} for first hydrogen on the Ti decorated 2D o-B_2N_2 is -0.47 eV, satisfying the DoE's criteria. Furthermore, the charge donation from the Ti atom to the 2D o-B_2N_2 was observed through PDOS, Löwdin charge analysis and CDD plot. The two Ti decorated configuration demonstrated the capacity to bind a total of thirty-four hydrogen molecules, with average E_{ad} of -0.31 eV/H_2 and 396 K of T_D. The calculated G_{SC}

(wt%) is 11.21%, notably surpassing the DoE's specified range. At a temperature of 396 K, our AIMD results convincingly demonstrate the excellent thermal stability of the Ti decorated 2D o-B_2N_2. As a summary, this research highlights the promising prospects of the Ti decorated 2D o-B_2N_2 as an efficient medium for high-capacity hydrogen storage. We are hoping that our theoretical prediction motivates the experimentalists to design 2D o-B_2N_2 based hydrogen storage medium.

References

1 A. Mikhaylov, N. Moiseev, K. Aleshin and T. Burkhardt, *Entrep. Sustain. Issues*, 2020, **7**, 2897–2913.

2 I. P. Jain, *Int. J. Hydrogen Energy*, 2009, **34**, 7368–7378.

3 B. Chettri, P. K. Patra, N. N. Hieu and D. P. Rai, Surfaces and Interfaces, 2021, **24**, 101043.

4 K. Jha, P. Gulati and U. K. Tripathi, U.K. (Eds.), Recent Advances in Sustainable Technologies: Select Proceedings of ICAST 2020, Springer, 2021.

5 A. Züttel, A. Remhof, A. Borgschulte and O. Friedrichs, *Philos. Trans. R. Soc. A Math. Phys. Eng. Sci.*, 2010, **368**, 3329–3342.

6 P. Prachi R., W. Mahesh M. and G. Aneesh C., *Adv. Energy Power*, 2016, **4**, 11–22.

7 H. T. Nair, P. K. Jha and B. Chakraborty, *Int. J. Hydrogen Energy*, 2022, DOI:10.1016/j.ijhydene.2022.08.084.

8 L.-P. Ma, Z.-S. Wu, J. Li, E.-D. Wu, W.-C. Ren and H.-M. Cheng, *Int. J. Hydrogen Energy*, 2009, **34**, 2329–2332.

9 V. Mahamiya, A. Shukla, N. Garg and B. Chakraborty, *Bull. Mater. Sci.*, 2022, **45**, 200.

10 Y. Liu, L. Ren, Y. He and H.-P. Cheng, *J. Phys. Condens. Matter*, 2010, **22**, 445301.

11 S. Chu, L. Hu, X. Hu, M. Yang and J. Deng, *Int. J. Hydrogen Energy*, 2011, **36**, 12324–12328.

12 S. Desnavi, B. Chakraborty and L. M. Ramaniah, *AIP Conf. Proc.*, 2014, **1591**, 1775–1777.

13 W. Liu, Y. Liu and R. Wang, *Appl. Surf. Sci.*, 2014, **296**, 204–208.

14 M. Zhou, Y. Lu, C. Zhang and Y. P. Feng, *Appl. Phys. Lett.*, 2010, **97**, 103109.

15 D. Kag, N. Luhadiya, N. D. Patil and S. I. Kundalwal, *Int. J. Hydrogen Energy*, 2021, **46**, 22599–22610.

16 J. Bao, K. Jeppson, M. Edwards, Y. Fu, L. Ye, X. Lu and J. Liu, *Electron. Mater. Lett.*, 2016, **12**, 1–16.

17 T. Wang, C. Wang, Y. Huo and M. Liu, *Chem. Phys. Lett.*, 2022, **803**, 139853.

18 P. Fu, J. Wang, R. Jia, S. Bibi, R. I. Eglitis and H.-X. Zhang, *Comput. Mater. Sci.*, 2017, **139**, 335–340.

19 X. Zhou, W. Chu, Y. Zhou, W. Sun and Y. Xue, *Appl. Surf. Sci.*, 2018, **439**, 246–253.

20 P. Banerjee, B. Pathak, R. Ahuja and G. P. Das, *Int. J. Hydrogen Energy*, 2016, **41**, 14437–14446.

21 M. Rafique, M. A. Uqaili, N. H. Mirjat, M. A. Tunio and Y. Shuai, *Phys. E Low-Dimensional Syst. Nanostructures*, 2019, **109**, 169–178.

22 H. Zhang, C.-J. Tong, Y. Zhang, Y.-N. Zhang and L.-M. Liu, *J. Mater. Chem. A*, 2015, **3**, 9632–9637.

23 R. Konda, A. Deshmukh, E. Titus and A. Chaudhari, *Int. J. Hydrogen Energy*, 2017, **42**, 23723–23730.

24 S. Demirci, S. E. Rad, S. Kazak, S. Nezir and S. Jahangirov, *Phys. Rev. B*, 2020, **101**, 1–5.

25 R. L. Kumawat and B. Pathak, *Appl. Surf. Sci.*, 2022, **586**, 152850.

26 N. Khossossi, W. Luo, Z. Haman, D. Singh, I. Essaoudi, A. Ainane and R. Ahuja, *Nano Energy*, 2022, **96**, 107066.

27 M. M. Kadhim, R. Kadhim Mahmood, N. Ali, Z. Sabri Abbas, S. K. Hachim, S. A. H. Abdullaha and A. Mahdi Rheima, *Comput. Theor. Chem.*, 2022, **1218**, 113935.

28 M. M. Kadhim, N. Sadoon, S. A. H. Abdullaha, Z. Sabri Abbas, A. Mahdi Rheima and S. K. Hachim, *Inorg. Chem. Commun.*, 2023, **151**, 110461.

29 D. Chodvadiya, M. H. Dalsaniya, N. N. Som, B. Chakraborty, D. Kurzydłowski, K. J. Kurzydłowski and P. K. Jha, *Int. J. Hydrogen Energy*, 2023, **48**, 5138–5151.

30 R. Rahimi and M. Solimannejad, *Energy and Fuels*, 2021, **35**, 6858–6867.

31 P. Giannozzi et al., *J. Phys. Condens. Matter*, 2009, **21**, 395502.

32 J. P. Perdew, K. Burke and Y. Wang, *Phys. Rev. B*, 1996, **54**, 16533–16539.

33 S. Grimme, *J. Comput. Chem.*, 2006, **27**, 1787–1799.

34 H. J. Monkhorst and J. D. Pack, *Phys. Rev. B*, 1976, **13**, 5188–5192.

35 V. Mahamiya, A. Shukla and B. Chakraborty, *Int. J. Hydrogen Energy*, 2022, **47**, 41833–41847.

36 G. Sanyal, H. T. Nair, P. K. Jha and B. Chakraborty, *J. Energy Storage*, 2023, **68**, 107892.

37 D. Chodvadiya, P. K. Jha and B. Chakraborty, *Int. J. Hydrogen Energy*, 2022, **47**, 41733–41747.

38 P. Panigrahi, A. Kumar, A. Karton, R. Ahuja and T. Hussain, *Int. J. Hydrogen Energy*, 2020, **45**, 3035–3045.

39 Y. Yong, Q. Hou, X. Yuan, H. Cui, X. Li and X. Li, *J. Energy Storage*, 2023, **72**, 108169.

40 P. Mane, S. P. Kaur, M. Singh, A. Kundu and B. Chakraborty, *Int. J. Hydrogen Energy*, 2023, **48**, 28076–28090.

41 B. Chakraborty, P. Ray, N. Garg and S. Banerjee, *Int. J. Hydrogen Energy*, 2021, **46**, 4154–4167.

42 B. Chettri, P. K. Patra, N. N. Hieu and D. P. Rai, *Surfaces and Interfaces*, 2021, **24**, 101043.

43 H. Liang, B. Cao, J. Zhu, X. Shen, M. Zhu, B. Geng, P. Zhang, S. Zhu, F. Yu, R. Zhang, H. Tang, Q. Yuan, J. Li, W. Li and Y. Chen, *Appl. Surf. Sci.*, 2022, **604**, 1–7.

44 J. Dewangan, V. Mahamiya, A. Shukla and B. Chakraborty, *Energy Storage*, 2023, **5**, e391.

45 M. R. Mananghaya, *Nanoscale*, 2019, **11**, 16052–16062.